RSC Advances

PAPER

View Article Online
View Journal | View Issue

Check for updates

Cite this: *RSC Adv.*, 2020, **10**, 44633

Pressure dependent half-metallic ferromagnetism in inverse Heusler alloy Fe_2CoAl: a DFT+U calculations

D. P. Rai, *[a] Lalrinkima,[ab] Lalhriatzuala,[a] L. A. Fomin,[c] I. V. Malikov,[c] Adlane Sayede,[d] Madhav Prasad Ghimire,*[e] R. K. Thapa[b] and Lalthakimi Zadeng[b]

We report the electronic and magnetic properties along with the Curie temperature (T_C) of the inverse full Heusler alloy (HA) Fe_2CoAl obtained by using the first-principles computational method. Our calculations suggests that Fe_2CoAl is a magnetic metal when treated within PBE-GGA under the applied compressive pressures. However, the implementation of electron–electron (U) (*i.e.*, GGA+U) with varying compressive pressure (*P*) drastically changes the profile of the electronic structure. The application of GGA+U along with pressure induces ferromagnetic half-metallicity with an integer value of total magnetic moment ~4.0 μ_B per unit cell. The integer value is in accordance with the Slater–Pauling's rule. Here, we demonstrate the variation of semiconducting gap in the spin down channel. The band gap increases from 0.0 eV to 0.72 eV when increasing the pressure from 0 to 30 GPa. Beyond 30 GPa, the electronic band gap decreases, and it is completely diminished at 60 GPa, exhibiting metallic behaviour. The analysis of the computed results shows that the treatment of electron–electron interactions within GGA+U and the application of compressive pressure in Fe_2CoAl enables d–d orbital hybridization giving rise to a half-metal ferromagnet. The T_C calculated from mean field approximation (MFA) decreases up to 30 GPa and then increases linearly up to 60 GPa.

Received 2nd September 2020
Accepted 5th November 2020

DOI: 10.1039/d0ra07543d

rsc.li/rsc-advances

Open Access Article. Published on 17 December 2020. Downloaded on 12/9/2025 9:53:01 AM.
This article is licensed under a Creative Commons Attribution 3.0 Unported Licence.

1 Introduction

The discovery of the prototype Heusler alloy Cu_2MnAl in 1903 (ref. 1) initiated new research interest due to its ferromagnetic behaviour despite having all non-magnetic constituents.[1,2] Heusler alloys have been studied for 120 years, but the application of these materials in spintronics has only been considered for 30–40 years.[3–12] Half-metal ferromagnetism (HMF) is the top priority among all the explored properties of Heusler alloys.[13–20] HMF occurs when magnetic materials exhibit metallic behavior in one of the spin channels whereas the other spin channel is semiconducting. Rigorous research has been performed in order to understand the underlying mechanism of unusual ferromagnetic behaviour in terms of atomistic scale interactions. Several theories and models have been proposed for the integration of these exotic properties in new technological applications in spintronics.[21] Spintronics is a branch of science which deals with the charge and spin of an electron. High capacity storage devices, magnetic RAM, spin-injection, spin-valves, spin-filters, GMR, TMR, and many more potential electron spin-based components are foreseen.[22–25] To improve the storage capacity of memory devices, the manipulation of spin degrees of freedom is crucial. Fabrication of practical devices with enhanced efficiency is another challenging task. Some of the Heusler alloys with high spin polarization and high Curie temperature[21,26] are promising and may complement this goal. Although the practical application of HMF in spintronic devices is in the preliminary stage, lab work is still in progress. Heusler alloys with 3d-orbitals are very sensitive to externally applied fields (temperature, pressure, electric and magnetic fields), and as a result their electronic and magnetic properties can be tuned very readily. The d–d orbital hybridization between the transition metals is reported to be responsible for some of their outstanding electronic and magnetic properties, including the high value of spin polarization at the Fermi level (E_F).[18] They exhibit low Gilbert damping, high Curie temperature, high spin polarization, *etc.*[27–37] In addition, Heusler alloys are also explored as potential thermoelectric materials[38] due to the presence of non-toxic components and their large range of working temperatures as compared to other thermoelectric

[a]*Physical Sciences Research Center, Department of Physics, Pachhunga University College, Aizawl 796001, India. E-mail: dibya@pucollege.edu.in*
[b]*Department of Physics, Mizoram University, Aizawl 796009, India*
[c]*Institute of Microelectronics Technology and High Purity Materials RAS, 142432 Chernogolovka, Russia*
[d]*Univ. Artois, CNRS, Centrale Lille, ENSCL, Univ. Lille, UMR 8181-UCCS-Unité de Catalyse et Chimie du Solide, F-62300 Lens, France*
[e]*Central Department of Physics, Tribhuvan University, Kathmandu, Nepal. E-mail: madhav.ghimire@cdp.tu.edu.np*

Open Access Article. Published on 17 December 2020. Downloaded on 12/9/2025 9:53:01 AM.
This article is licensed under a Creative Commons Attribution 3.0 Unported Licence.

materials.[39–42] Currently, numerous theoretical and experimental research investigations are in progress to study the electronic and magnetic properties of Heusler alloys *via* structural modifications under applied strain and hydrostatic pressure. Under applied hydrostatic pressure, the bond lengths vary due to the displacement of atoms from their mean positions and changes electronic charge densities which have a direct impact on the electronic and magnetic properties.[43,44] Ram *et al.* have reported significant changes in the band structure of Co_2XY (X = Cr, Mn and Y = Al, Ga) type direct full-Heusler alloys under applied pressure.[45] Rasul *et al.*[46] have studied the quaternary Heusler alloys ScNiCrX (X = Al, Ga) using a first-principles approach and reported the robustness of the half-metallicity up to 6 GPa and 16 GPa for ScNiCrAl and ScNiCrGa, respectively. Amudhavalli *et al.*[47] studied Fe-based ferromagnetic quaternary Heusler alloys and reported a pressure induced structural phase transition at 151.6 GPa, 33.7 GPa, 76.4 GPa, 85.3 GPa, 87.7 GPa and 96.5 GPa for CoFeTiSi, CoFeTiGe, CoFeTiAs, NiFeTiSi, NiFeTiGe and NiFeTiAs, respectively. The same group,[48] performing similar kinds of studies, have reported a half-metal to metal phase transition for Co_2TiAl, Co_2TiGa and Co_2TiIn under applied external pressures of 76.5 GPa, 73.1 GPa and 63.9 GPa, respectively. Rambabu *et al.* studied the variation of the Curie temperature (T_C) under applied pressure and reported enhanced T_C at high compressive pressures.[49] There are reports on the variation of T_C of various Heusler alloys (such as Ni–Mn based alloys) under applied pressure.[50–52] Dannenberg *et al.*[53] reported the structural dependence of T_C of Fe_2CoGa: ~780 K for $L2_1$ and ~770 K for $L1_0$, respectively. Some more promising results for T_Cs for Fe-based full-Heusler alloys[54] under ambient conditions are: 925 K (Fe_2CoGe), 750 K (Fe_2NiGe), 845 K (Fe_2NiGa), 798 K (Fe_2CuGa), and 875 K (Fe_2CuAl). In our previous work[55] only Co_2FeAl exhibited half-metallicity with the implementation of DFT+U whereas Fe_2CoAl was metallic. However, there is a pseudo bandgap above the Fermi energy in the spin-down channel of Fe_2CoAl within DFT+U. Thus we were encouraged to implement external pressure to observe the location of the bandgap. Interestingly, we have observed a projection of the bandgap in the Fermi level in the spin-down channel, giving rise to half-metallicity. Therefore, we have applied pressure, which shortens the bond lengths and facilitates d–d hybridization, which may give the desired results. In this paper, we have also tried to explore the electronic and magnetic properties along with the T_C under compressive pressure using the first-principles approach. We report the sensitiveness of the electronic and magnetic properties under lattice strain due to applied pressure.

2 Computational details

In terms of their chemical compositions, Heusler alloys are classified as binary (X_3Z), ternary (X_2YZ or XYZ), and quaternary (AXYZ) compounds, where A, X and Y are transition metals and Z is a p-block element. Binary HAs only have two distinguishable elements in the unit cell. In general, ternary HAs are of two types *viz.* full (X_2YZ) and half (XYZ) HAs. The stoichiometric atomic ratios of full (X_2YZ) and half (XYZ) ternary HAs are 2 : 1 : 1 and 1 : 1 : 1, respectively. On the other hand, quaternary HAs have an equiatomic stoichiometric ratio of 1 : 1 : 1 : 1. Herein, we focus on ternary full-HAs. Ternary full-HAs crystallize in two ordered phases: Cu_2MnAl-type with space group $Fm\bar{3}m$ (225)[35,56] and Hg_2CuTi-type with the $F\bar{4}3m$ (216) space group.[57,58] The former is referred to as regular/direct ($L2_1$) and the latter is inverse/indirect with XA-structure. The atomic Wyckoff positions for both the XA-phase and the $L2_1$-phase of Fe_2CoAl are tabulated in Table 1. In the case of ternary inverse full-HAs the electronegativity of the X-atom is less than that of the Y-atom (X = Fe and Y = Co). Thus, our Fe_2CoAl system is an inverse full-HA with the electronegativity of the Fe-atom being less than that of the Co-atom. The primitive and conventional unit cells of Fe_2CoAl with XA-structure are shown in Fig. 1. To study the electronic and magnetic properties of the inverse full-Heusler alloy Fe_2CoAl, we have performed first-principles Density Functional Theory (DFT) calculations.[59,60] All electron–electron interactions were considered according to the generalized gradient approximation (GGA) within the Perdew–Burke–Ernzerhof (PBE) parametrization.[61] We are aware that GGA is inadequate for treating strongly correlated d-electrons to derive accurate electronic structures. On the other hand, the successful obtainment of accurate electronic properties by using GGA+U has already been reported for many Heusler alloys.[62–67] Therefore, we have applied a screened Coulomb interaction along with the conventional GGA (GGA+U or DFT+U) in order to

Table 1 Wyckoff positions of the Fe_2-based inverse full-Heusler alloy Fe_2CoAl

Positions	*x*	*y*	*z*
Inverse			
Fe1	0.75	0.75	0.75
Fe2	0.50	0.50	0.50
Co	0.25	0.25	0.25
Al	0.00	0.00	0.00
Direct			
Fe1	0.25	0.25	0.25
Fe2	0.75	0.75	0.75
Co	0.50	0.50	0.50
Al	0.00	0.00	0.00

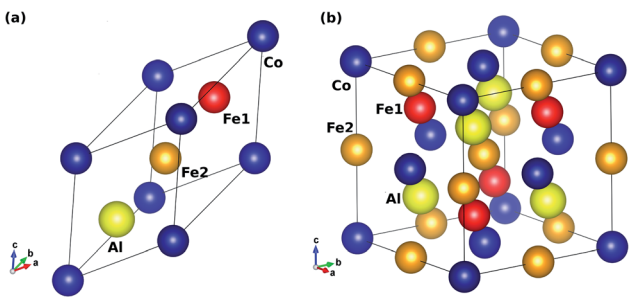

Fig. 1 (a) Primitive and (b) conventional unit cell of the inverse Heusler alloy Fe_2CoAl with space group $F\bar{4}3m$. Balls in red, orange, blue and yellow in the represents Fe1, Fe2, Co and Al respectively.

 This journal is © The Royal Society of Chemistry 2020

Open Access Article. Published on 17 December 2020. Downloaded on 12/9/2025 9:53:01 AM.
This article is licensed under a Creative Commons Attribution 3.0 Unported Licence.

deal with strongly correlated 3d electrons.[68] We have adopted U parameters of 3.82 eV for Fe and 3.89 eV for Co according to our previous work.[55,69] For computation, we have used the all electron orbital based full potential linearized augmented plane wave (FP-LAPW) basis set formalism as implemented in the WIEN2K package.[70] The non-spherical cut off value of angular momentum within the muffin tin (MT) sphere is $l_{max} = 10$. $R_{MT} \times K_{max} = 7$ where K_{max} is the maximum value of the reciprocal lattice vector in the plane wave expansion and R_{MT} is the smallest muffin tin (MT) radius. To model the electronic structure, the first Brillouin zone (BZ) was integrated by taking a $10 \times 10 \times 10$ k-mesh grid within the Monkhorst package. The self-consistency convergence criterion was set to be 0.0001 Ry. The ferromagnetic–antiferromagnetic exchange energy J_{ij} is a key parameter in determining the Curie temperature (T_C). A code based on the single-site coherent potential approximation within the Green's function approach called spin-polarized relativistic Korringa–Kohn–Rostoker (SPR-KKR)[71,72] was used for the calculation of T_C.

3 Results and discussion

3.1 Structural properties

Our first-principles calculations start with the optimization of both the $L2_1$ (direct) and XA (inverse) structures with different magnetic configurations. The initial magnetic configurations set for our calculations are ferromagnetic FM (Fe1↑, Fe2↑, Co↑), antiferromagnetic AFM1 (Fe1↑, Fe2↓, Co↑), and AFM2 (Fe1↑, Fe2↑, Co↓) (see Table 2). The variations in total energy *versus* the lattice constant a (Å) for both the direct and inverse phases with the FM, AFM1 and AFM2 magnetic configurations are shown in Fig. 2a and b. The XA-structure (inverse) with the FM configuration is energetically favourable with the minimum energy as shown by the blue line and the diamonds [see Fig. 2b]. The ground state energy and pressure as a function of volume are also presented in Fig. 2c and d. The calculated lattice constant is 5.73 Å and is consistent with previously reported values of 5.70 Å,[73] 5.71 Å,[74] 5.766 ± 0.05 Å,[75] and 5.732 Å.[76] This result also agrees well with the results for several other analogous Fe-based inverse Heusler alloys whose lattice parameters vary from 5.5 to 6.2 Å.[35,54,55,77–84] Further, the cohesive energy has been calculated from eqn (1). The cohesive energy results are presented in Fig. 7c and confirm the ground state stability of each system under different applied pressures.

Table 2 Magnetic configuration (MC) of the individual atoms Fe1, Fe2, Co, and Al, and total ground state energy E_T in Ry

MC	Fe1	Fe2	Co	Al	E_T
Inverse					
FM	↑	↑	↑	N	−1074.852
AFM1	↑	↓	↑	N	−1074.829
AFM2	↑	↑	↓	N	−1074.8509
Direct					
FM	↑	↑	↑	N	−1074.818
AFM1	↑	↓	↑	N	−1074.792
AFM2	↑	↑	↓	N	−1074.758

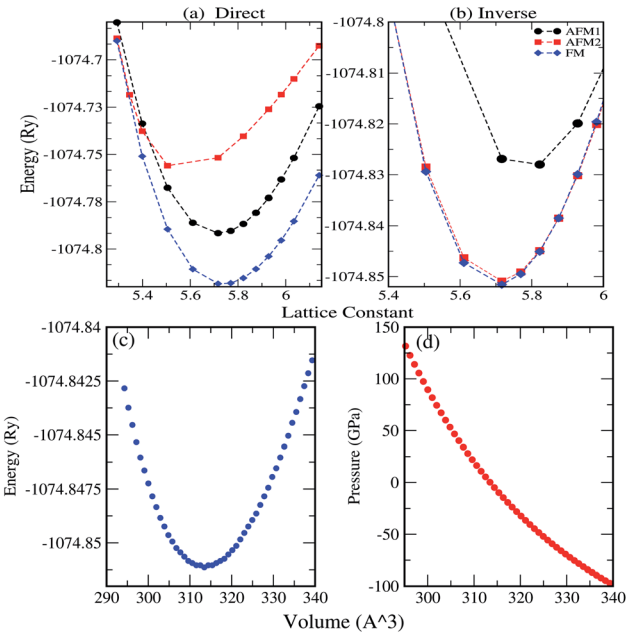

Fig. 2 Variation of total energy as a function of lattice constant a (Å): (a) direct phase, (b) inverse phase (AMF1, AFM2 and FM configurations are represented by black, red and blue lines, respectively), (c) ground state energy as a function of volume in Å^3 for FM and (d) pressure in GPa as a function of volume in Å^3.

$$E_C = \frac{E_{Fe1} + E_{Fe2} + E_{Co} + E_{Al} - E_T}{4} \quad (1)$$

Here in eqn (1), E_{Fe1}, E_{Fe2}, E_{Co}, E_{Al} and E_T are the individual energies of Fe1, Fe2, Co, and Al, and the total energy of the system, respectively. $n = 4$ denotes the total number of atoms in the unit cell.

3.2 Electronic and magnetic properties

We have investigated the electronic properties of Fe_2CoAl by calculating the total density of states (TDOS) and energy bands at different pressures using GGA+U [*cf.* Fig. 3–5]. We have already reported the inadequacy of GGA in deriving the electronic properties in our previous work.[55] On the other hand, GGA+U has predicted a band gap in the spin down channel but this is well above the Fermi level (E_F). We have observed the presence of some band edges at the E_F, mostly originating from Fe1-d (t_{2g}), Fe2-d (e_g, t_{2g}) and Co-d (e_g, t_{2g}) [*cf.* Fig. 4a–d]. However, the Fe1-d (e_g) state is hardly seen in the picture as it lies far below the E_F in the spin up channel [*cf.* Fig. 4a]. Hence, we have proceeded with our calculations by using GGA+U along with the application of compressive pressure. Interestingly, on the application of compressive pressure (5 GPa), the E_F is pushed upward within the band gap [Fig. 3a and b]. The half-metallic band gap is attributed to the d–d hybridization between Fe2-d and Co-d followed by Fe1-d states to give bonding–antibonding states as in the case of other full-Heusler alloys.[15–19,26] The bonding states at the top of the valence band

Open Access Article. Published on 17 December 2020. Downloaded on 12/9/2025 9:53:01 AM.
This article is licensed under a Creative Commons Attribution 3.0 Unported Licence.

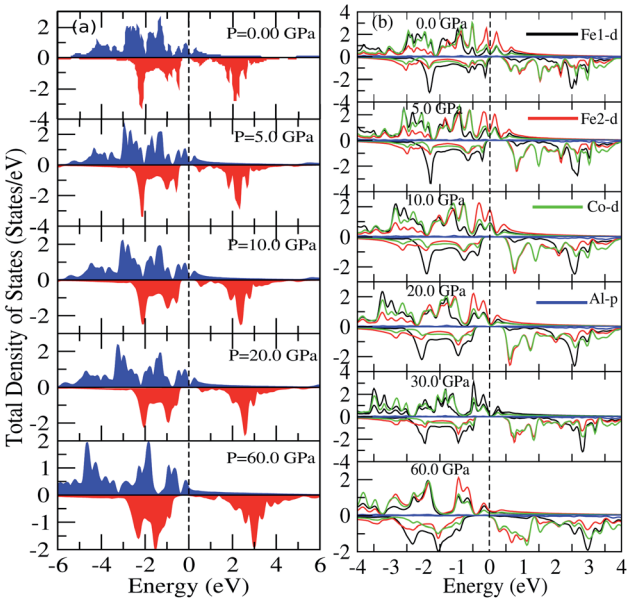

Fig. 3 (a) Total DOS calculated using GGA+U, (b) partial DOS of Fe1-d, Fe2-d, Co-d and Al-p calculated with GGA+U at different pressures.

form the valence band maximum (VBM) and the lowest anti-bonding states in the conduction region form the conduction band minimum (CBM). On the other hand, the spin up channel is still conducting. This hybrid characteristic of being semi-conducting in the spin down channel and conducting in the spin up channel results in peculiar half-metal ferromagnetic (HMF) behaviour. We have also noticed widening of the band gap with increasing compressive pressure, as this facilitates hybridization due to shortening of the bond lengths. The energy band gap increases from 0.0 eV to 0.72 eV on increasing the pressure from 0 to 30 GPa [*cf.* Fig. 7d]. This result can also be confirmed by the energy band structure which exhibits the indirect nature of the band gap as measured along the L–X symmetry and denoted by the green circles [*cf.* Fig. 5]. In Fig. 3 and 4, we observe a large band gap of ~0.72 eV at 30 GPa with the E_F pinned exactly in the middle of the band gap, providing more evidence of half-metallicity. A further increase in applied pressure (say beyond 30 GPa) decreases the band gap with drifting of the upper band edge (CBM) towards lower energy (specifically towards the E_F). This can be seen in Fig. 3b and 4a–d in which the Fe1-d state has moved towards higher energy in the conduction band, taking part less in the d–d hybridization, and the coupled Fe2-d–Co-d bands are pushed towards lower energy (*i.e.* towards the E_F) in the spin down region. It looks like the E_F shifts from the lower to the upper edge of the half-metallic band gap in the spin down channel on increasing the pressure, a typical feature of band flip. At 60 GPa the CBM (upper edge of the band gap) appears at the E_F, thus diminishing the half-metallic behaviour and increasing the metallicity. The robustness of the half-metallicty is measured in terms of spin polarization at the E_F. The degree of spin polarization in the vicinity of the E_F can be analyzed by $P = [N_\uparrow(E_F) - N_\downarrow(E_F)]/[N_\uparrow(E_F) + N_\downarrow(E_F)]$, where $N_\uparrow(E_F)$ and $N_\downarrow(E_F)$ are the numbers of states at E_F for the spin up and spin down channels, respectively. Our GGA+U calculation with pressure has significantly improved the spin polarization by more than 45%. At 5 GPa we estimated ~98% spin polarization. On varying the pressure, $5 < P < 60$ GPa, we have achieved perfect half-metallic behaviour in our Fe_2CoAl system. The projection of E_F inside the band gap in the spin down channel and the finite value of the electron density around E_F in the spin up channel at $5 < P < 60$ GPa results in 100% spin polarization. To analyse the nature of the bonding between the atoms we have calculated the valence electron charge density (e $Å^{-3}$) and the results at 30 GPa are presented in Fig. 6. The analysis of the charge density shows the presence of metallic bonding between the atoms and no sign of covalent bonds.

As reported elsewhere, the magnetic properties of perfect half-metallic ferromagnet (HMF) Heusler alloys (HAs) can be

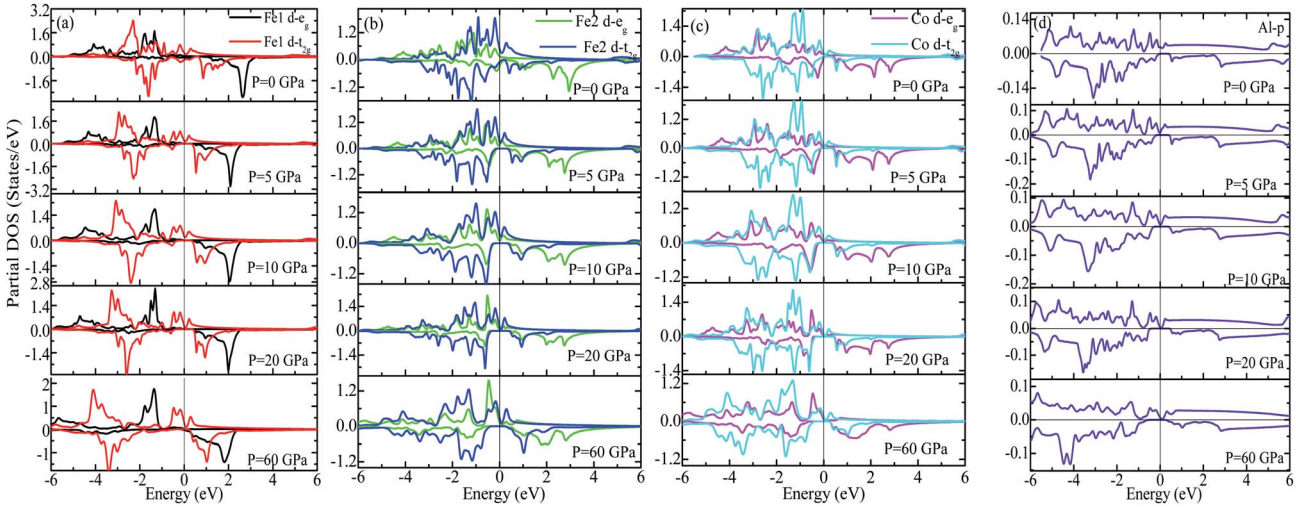

Fig. 4 (a) Partial DOS of Fe1 (d-e_g, d-t_{2g}), (b) partial DOS of Fe2 (d-e_g, d-t_{2g}), (c) partial DOS of Co (d-e_g, d-t_{2g}) and (d) partial DOS of Al-p at different pressures.

This journal is © The Royal Society of Chemistry 2020

Open Access Article. Published on 17 December 2020. Downloaded on 12/9/2025 9:53:01 AM.
This article is licensed under a Creative Commons Attribution 3.0 Unported Licence.

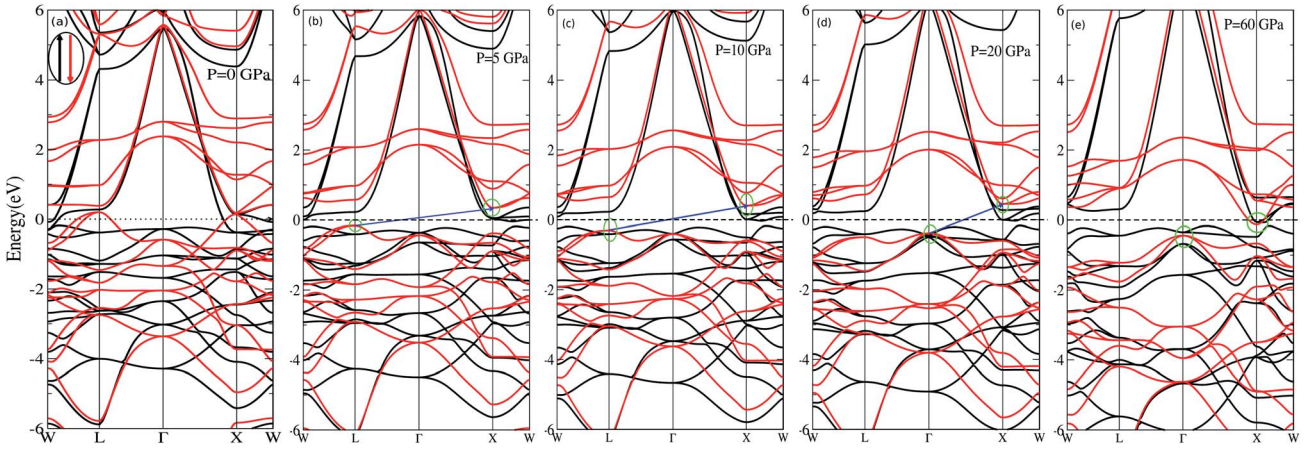

Fig. 5 Band energies of Fe_2CoAl calculated with GGA+U at (a) $P = 0$ GPa, (b) $P = 5$ GPa, (c) $P = 10$ GPa, (d) $P = 20$ GPa and (e) $P = 60$ GPa.

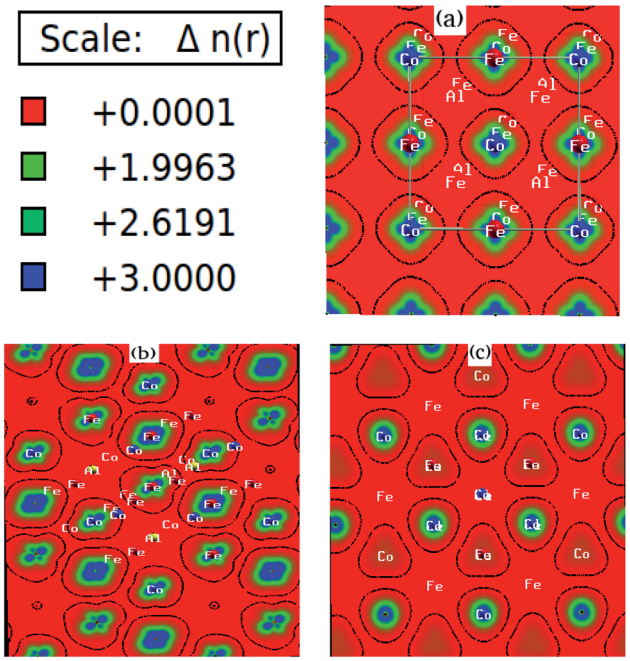

Fig. 6 Electron density (e Å^{-3}) of Fe_2CoAl along the (a) 001, (b) 011 and (c) 111 directions.

predicted from the total number of valence electrons present in the unit cell.[15–18,26] The total magnetic moment can be derived from the Slater–Pauling (SP) rule[18] as given by $M_t = (Z_t - 24)\ \mu_B$, where M_t is the total magnetic moment and Z_t is the total number of valence electrons. The total number of valence electrons in our Fe_2CoAl system is $2 \times 8 + 9 + 3 = 28$. So the expected value of the total magnetic moment is $M_t = 4.0\ \mu_B$ which results in the half-metallicity. The total magnetic moment obtained from GGA sharply deviates from the Slater–Pauling rule. However, on treating the system within GGA+U and applying pressures (0–70 GPa), the total magnetic moment M_t varies around 4.0 μ_B. The highest $M_t = 4.440\ \mu_B$ and the lowest $M_t = 3.981\ \mu_B$, calculated at 0 GPa and 70 GPa, respectively [Table 3]. The M_t values at 0 and 70 GPa do not comply

Table 3 Total and partial magnetic moments (in μ_B) calculated with GGA+U along with the Curie temperature T_C (in K)

P (GPa)	M_{Tot}	M_{Fe1}	M_{Fe2}	M_{Co}	T_C^{cal}	T_C^{MFA}
0.0	4.440	2.126	1.011	1.109	826.640	1164.30
5.0	4.030	2.158	0.989	1.075	752.430	1134.90
10.0	3.999	2.171	0.990	1.051	746.819	1130.60
20.0	3.990	2.165	1.010	1.018	745.190	1127.20
30.0	4.000	2.155	1.016	0.995	747.000	1124.20
40.0	3.996	2.152	1.009	0.979	744.828	1146.30
50.0	4.009	2.137	1.025	0.978	748.629	1173.50
60.0	3.988	2.121	1.028	0.964	746.276	1190.40
70.0	3.981	2.105	1.024	0.957	743.561	1187.00

with the SP rule. Also, at 60 GPa $M_t = 3.988\ \mu_B$ and $\Delta\mu_B = \sim 0.012$ or ~0.3%. At applied pressures of $5 < P < 60$ GPa, the M_t value is ~4 μ_B. Thus, we can claim that the M_t values are in accordance with the SP rule[18] at $5 < P < 60$ GPa. We also present the variation of the partial magnetic moments calculated with GGA and

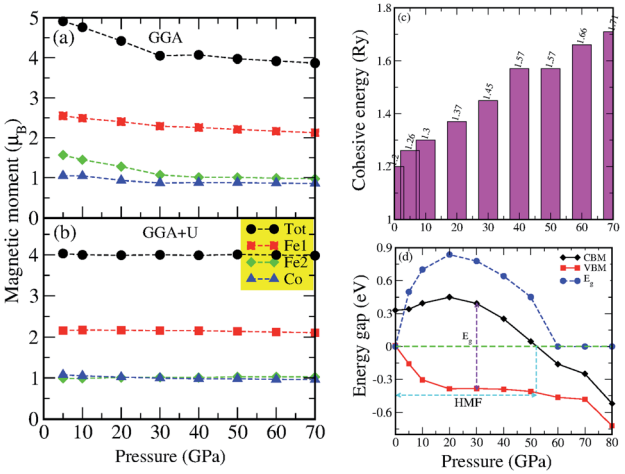

Fig. 7 (a and b) Total and partial magnetic moments calculated with the FPLAPW method using WIEN2K, variation of (c) cohesive energy and (d) energy band gap as a function of pressure.

Open Access Article. Published on 17 December 2020. Downloaded on 12/9/2025 9:53:01 AM.
This article is licensed under a Creative Commons Attribution 3.0 Unported Licence.

GGA+U under different pressures in Fig. 7a and their numerical values are tabulated in Table 3.

In order to further understand the magnetic interactions and magnetic properties, we have calculated the magnetic exchange energy by modeling the pair exchange interaction parameter J_{ij}. The J_{ij} parameter is computed using the Heisenberg model.[17] The exchange coupling interactions are mapped between the atoms sitting at the i and j sites separated by some distance as in eqn (2)

$$J_{ij} = \frac{1}{4\pi}\int_{E_F} d(E)\mathrm{Tr}_L\{\Delta_i T_\uparrow^{ij}\Delta_j T_\uparrow^{ji}\}, \quad (2)$$

where $\Delta_i = t_{i\uparrow}{}^{-1} - t_{j\downarrow}{}^{-1}$, $t_{\uparrow\downarrow}{}^{-1}$ is the atomic t-matrix of the magnetic impurities at site i for the spin up/down state, $T_{\uparrow\downarrow}^{ij}$ is the scattering path operator between the i and j sites for the spin up/down state, and Tr_L is the trace over the orbital variables of the scattering matrices. The calculated exchange parameters J_{ij} for a central Fe1 atom interacting with all other atoms (Al–Fe1, Fe1–Fe1, Fe2–Fe1 and Co–Fe1) as a function of R_{ij}/a at different pressures are shown in Fig. 8a–d. The estimated J_{ij} is a key parameter for obtaining the Curie temperature (T_C) in the mean-field approximation (MFA) as given in eqn (3):

$$k_B T_C^{MFA}\langle s_i\rangle = \frac{2}{3}c\sum_{j,r\neq 0} J_{ij}{}^{0,r}\langle s_j\rangle, \quad (3)$$

where k_B is the Boltzmann constant, c is the concentration of the impurities, and $\langle s_j\rangle$ is the average j component of the unit vector $s_r{}^j$ along the direction of magnetization. The J_{ij} below $R_{ij}/a = \sim 1$ (below 1) shows a finite stable value. Meanwhile, the J_{ij} values above $R_{ij}/a = \sim 1$ (above 1) either remain close to 0 meV or fluctuate around 0 meV [*cf.* Fig. 8a–d]. The variation of the total J_{ij} along with the calculated T_C^{MFA} as a function of R_{ij}/a under

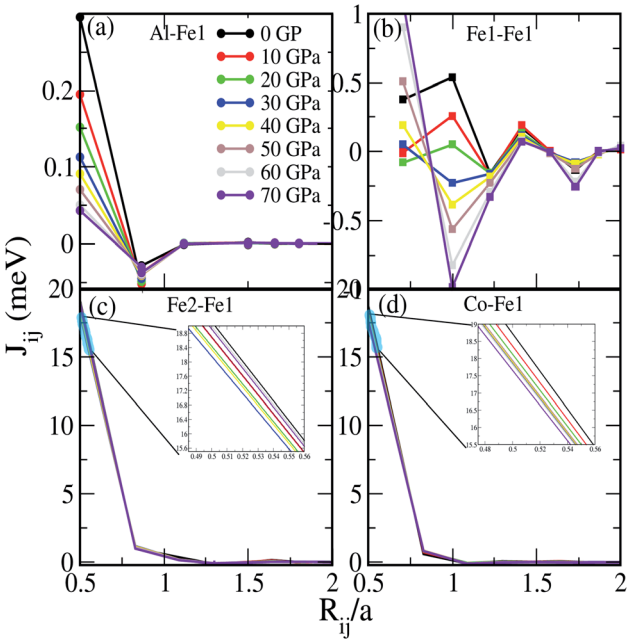

Fig. 8 Exchange interaction J_{ij} (meV) between (a) Al and Fe1, (b) Fe1 and Fe1, (c) Fe2 and Fe1 and (d) Co and Fe1 at different pressures.

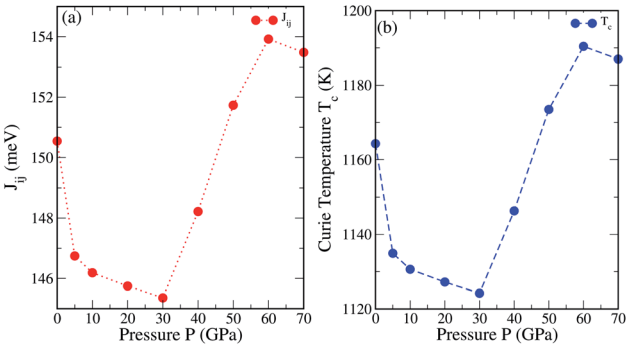

Fig. 9 (a) Exchange interaction J_{ij} (meV) and (b) Curie temperature T_C^{MFA} (K) as a function of pressure.

different pressures are shown in Fig. 9a and b. We can see that on increasing the pressure up to 30 GPa the J_{ij} parameter decreases systematically. This leads to a decrease in T_C^{MFA}. As shown in Fig. 8c the J_{ij} value is governed by a strong interaction between Fe1 and Fe2. The lowest calculated value of $T_C^{MFA} = 1124.20$ K at 30 GPa is mainly attributed to the low value of J_{ij} due to the short range ($R_{ij}/a < \sim 1$) interaction between Fe1 and Fe2 [see inset (blue line) in Fig. 8c]. For the Al–Fe1, Fe1–Fe1 and Co–Fe1 interactions, the J_{ij} values are intermediate at 30 GPa [*cf.* Fig. 8a–d]. On increasing the pressure beyond 30 GPa there occurs a linear increase in T_C^{MFA}, which reaches a maximum at 60 GPa. Our results for T_C^{MFA} contradict with the results of Rambabu *et al.* for Co_2CrX (X = Al, Ga, In) below 30 GPa, whereas at high pressure, *i.e.*, above 30 GPa they follow a similar trend.[49] The calculated T_C values obtained from the mean field approximation are tabulated in Table 3. The other method to estimate the T_C in relation to the total magnetic moment (M_t) of HMF-HAs is given by eqn (4).[19,26]

$$T_C^{cal} = 23 + 181 \times M_t \quad (4)$$

As we have already discussed the inefficiency of GGA in deriving the half-metallicity, estimating T_C by taking the M_t obtained from GGA is not justifiable. Therefore, we have taken the M_t values calculated with GGA+U and substituted in eqn (4) to obtain the T_C^{cal}. The estimated values of T_C^{cal} are presented in Table 3. The T_C^{cal} values vary from 826.640 K to 743.561 K on varying the pressure from 0 to 70 GPa. These results are in good agreement with the T_Cs of other analogous Fe-based inverse full-HAs.[54] We have noted that the T_C obtained from eqn (4) appears to be independent of interaction strength as the variation of the total magnetic moment (M_t) is very small. Referring to Table 3, the T_C values calculated with the MFA (eqn (3)) look much higher as compared to those calculated with eqn (4). The large values of T_C^{MFA} may arise due to inability to include the magnetic percolation effect within the mean field approximation.[55]

4 Conclusion

In summary, we have studied the structural, electronic and magnetic properties of the inverse HA Fe_2CoAl along with the T_C

This journal is © The Royal Society of Chemistry 2020

Open Access Article. Published on 17 December 2020. Downloaded on 12/9/2025 9:53:01 AM.
This article is licensed under a Creative Commons Attribution 3.0 Unported Licence.

values obtained from GGA and GGA+U under applied pressures. We have shown that the strong correlation mainly comes from the Fe-3d and Co-d states, and the inclusion of electron–electron interactions within GGA as the GGA+U formalism is essential to describe the electronic properties. The implementation of GGA+U along with compressive pressure ($5 < P < 60$ GPa) leads to half-metallic behavior with the opening of a spin minority band gap. The predicted integer value of the total magnetic moment in the inverse full-Heusler alloy Fe_2CoAl, $\sim$4.0 μ_B at 30 GPa, is in accordance with the Slater–Pauling rule, which supports the half-metallicity. The T_C calculated from eqn (4) is 747 K at 30 GPa, in good agreement with the results of other Fe-based inverse full-HAs. However, the results from MFA are overestimated.

Conflicts of interest

There are no conflicts to declare.

Acknowledgements

D. P. R. acknowledges the Department of Science and Technology New Delhi, Govt of India *vide* Lett. No. INT/RUS/RFBR/P-264. I. V. M. acknowledges the Russian Foundation for Basic Research (RFBR), Russia, RFBR-17-57-45024. M. P. G. thanks the Alexander von Humboldt Foundation for the equipment subsidy grants. D. P. R. extends condolences to the family of Prof. G. M. Mikhailov, an Indo-Russian project collaborator.

Notes and references

1 F. Heusler, W. Starck and E. Haupt, *Verh. Dtsch. Phys. Ges.*, 1903, **5**, 220–223.
2 O. Heusler, *Ann. Phys.*, 1934, **411**(2), 155.
3 D. C. Price, *J. Phys. F: Met. Phys.*, 1978, **8**, 933.
4 J. Kubler, A. R. Williams and C. B. Sommers, *Phys. Rev. B: Condens. Matter Mater. Phys.*, 1983, **28**, 1745.
5 J. L. Moran-Lapeza, R. Rodriguez-Albab and F. Aguilera-Granja, *J. Magn. Magn. Mater.*, 1994, **131**, 417.
6 E. Sasioglu, L. M. Sandratskii, P. Bruno and I. Galanakis, *Phys. Rev. B: Condens. Matter Mater. Phys.*, 2005, **72**, 184415.
7 J. Thoene, S. Chadov, G. Fecher, C. Felser and J. Kubler, *J. Phys. D: Appl. Phys.*, 2009, **42**, 084013.
8 S. Trudel, O. Gaier, J. Hamrle and B. Hillebrands, *J. Phys. D: Appl. Phys.*, 2010, **43**, 193001.
9 D. P. Rai, J. Hashemifar, M. Jamal, *et al.*, *Indian J. Phys.*, 2010, **84**, 717–721.
10 D. P. Rai, Sandeep, M. P. Ghimire, *et al.*, *Bull. Mater. Sci.*, 2011, **34**, 1219–1222.
11 S. Roy, N. Khan, R. Singha, A. Pariari and P. Mandal, *Phys. Rev. B*, 2019, **99**, 214414.
12 I. V. Malikov, L. A. Fomin, V. A. Berezin, A. V. Chernykh, D. P. Rai and G. M. Mikhailov, *Ferroelectrics*, 2019, **541**(1), 79–92.
13 R. A. de Groot, F. M. Mueller, P. G. van Engen and K. H. J. Buschow, *Phys. Rev. Lett.*, 1983, **50**, 2024.
14 K. H. J. Buschow and P. G. van Engen, *J. Magn. Magn. Mater.*, 1981, **25**, 90–96.
15 H. Kandpal, G. Fecher, C. Felser and G. Schonhense, *Phys. Rev. B: Condens. Matter Mater. Phys.*, 2006, **73**, 094422.
16 C. Felser, L. Wollmann, S. Chadov, G. Fecher and S. Parkin, *APL Mater.*, 2015, **3**, 041518.
17 A. Liechtenstein, M. Katsnelson, V. Antropov and V. Gubanov, *J. Magn. Magn. Mater.*, 1987, **67**(1), 65–74.
18 I. Galanakis, E. Sasıoglu and K. Ozdogan, *Phys. Rev. B: Condens. Matter Mater. Phys.*, 2014, **90**, 064408.
19 X. Q. Chen, R. Podloucky and P. Rogl, *J. Appl. Phys.*, 2006, **100**, 113901.
20 A. Bansil, S. Kaprzyk and J. Tobola, *Phys. Rev. B: Condens. Matter Mater. Phys.*, 1999, **60**, 13396.
21 A. Fert, *Thin Solid Films*, 2008, **517**, 2.
22 L. Xingxing and Y. Jinlong, *Natl. Sci. Rev.*, 2016, **3**, 365.
23 I. Galankis, K. Ozdogan and E. Sasioglu, *AIP Adv.*, 2016, **6**, 055606.
24 A. Planes, L. Manosa and M. Acet, *J. Phys.: Condens. Matter*, 2009, **21**, 233201.
25 P. Entel, V. D. Buchelnikov, V. V. Khovailo, A. T. Zayak, W. A. Adeagbo, M. E. Gruner, H. C. Herper and E. F. Wassermann, *J. Phys. D: Appl. Phys.*, 2006, **39**, 865.
26 S. Wurmehl, G. H. Fecher, H. C. Kandpal, V. Ksenofontov, C. Felser and H.-J. Lin, *Appl. Phys. Lett.*, 2006, **88**(3), 032503.
27 L. Bainsla and K. Suresh, *Appl. Phys. Lett.*, 2016, **3**, 031101.
28 X. Wang, Z. Cheng, J. Wang, X. Wang and G. Liu, *J. Mater. Chem. C*, 2016, **4**, 7176–7192.
29 T. Graf, C. Felser and S. Parkin, *Prog. Solid State Chem.*, 2011, **39**, 1–50.
30 S. Sanvito, C. Oses, J. Xue, A. Tiwari, M. Zic, T. Archer, P. Tozman, M. Venkatesan, M. Coey and S. Curtarolo, *Sci. Adv.*, 2017, **3**(4), e1602241.
31 D. Bensaid, T. Hellal, M. Ameri, Y. Azzaz, B. Doumi, Y. Al-Douri, B. Abderrahim and F. Benzoudji, *J. Supercond. Novel Magn.*, 2016, **29**, 1843–1850.
32 I. Yahiaoui, A. Lazreg, Z. Dridi, Y. Al-Douri and B. Bouhafs, *J. Supercond. Novel Magn.*, 2017, **30**, 421–424.
33 F. Semari, F. Dahmane, N. Baki, Y. Al-Douri, S. Akbudak, G. Ugur, S. Ugur, A. Bouhemadou, R. Khenata and C. H. Voon, *Chin. J. Phys.*, 2018, **56**, 567–573.
34 F. Khelfaoui, M. Ameri, D. Bensaid, I. Ameri and Y. Al-Douri, *J. Supercond. Novel Magn.*, 2018, **31**, 3183–3192.
35 D. P. Rai, Sandeep, A. Shankar, R. Khenata, A. H. Reshak, C. E. Ekuma, R. K. Thapa and S.-H. Ke, *AIP Adv.*, 2017, **7**(4), 045118.
36 D. Wu, Z. Zhe, L. Li, Z. Zhang, H. Zhao, J. Wang, B. Ma and Q. Jin, *Sci. Rep.*, 2015, **5**, 12352.
37 L. D. M. Shaughnessy, R. Snow and C. Y. Fong, *Phys. Rev. A: At., Mol., Opt. Phys.*, 2011, **2011**, 140805.
38 O. Appel and Y. Gelbstein, *J. Electron. Mater.*, 2014, **43**(6), 1976–1982.
39 Y. Gelbstein, *J. Electron. Mater.*, 2011, **40**(5), 533–536.
40 Y. Gelbstein, J. Davidow, E. Leshem, O. Pinshow and S. Moisa, *Phys. Status Solidi B*, 2014, **251**(7), 1431–1437.
41 G. M. Guttmann, D. Dadon and Y. Gelbstein, *J. Appl. Phys.*, 2015, **118**, 065102.

Open Access Article. Published on 17 December 2020. Downloaded on 12/9/2025 9:53:01 AM.
This article is licensed under a Creative Commons Attribution 3.0 Unported Licence.

42 G. Komisarchik, D. Fuks and Y. Gelbstein, *J. Appl. Phys.*, 2016, **120**(5), 055104.
43 T. Ouahrani, *Eur. Phys. J. B*, 2013, **86**, 369.
44 M. Marques, G. J. Ackland, L. F. Lundegaard, G. Stinton, R. J. Nelmes, M. I. McMahon and C. J. Garcia, *Phys. Rev. Lett.*, 2009, **103**, 115501.
45 S. Ram, M. R. Chauhan, K. Agarwal and V. Kanchana, *Philos. Mag. Lett.*, 2011, **91**, 545.
46 M. N. Rasul, A. Javed, M. A. Khan and A. Hussain, *Mater. Chem. Phys.*, 2019, **222**, 321–332.
47 A. Amudhavalli, R. Rajeswarapalanichamy and K. Iyakutti, *J. Magn. Magn. Mater.*, 2017, **441**, 21–38.
48 A. Amudhavalli, R. Rajeswarapalanichamy and K. Iyakutti, *Phase Transitions*, 2019, **92**, 875–887.
49 P. Rambabu, B. Anuroopa, M. Manivel Raja and V. Kanchana, *Solid State Sci.*, 2020, **105**, 106257.
50 E. Sasioglu, L. M. Sandratskii and P. Bruno, *Phys. Rev. B: Condens. Matter Mater. Phys.*, 2005, **71**, 214412.
51 B. Hamri, B. Abbar, A. Hamri, O. Baraka, A. Hallouche and A. Zaoui, *Comput. Condens. Matter*, 2015, **3**, 14.
52 X. P. Wei, Y. D. Chu, X. W. Sun, J. B. Deng and Y. Z. Xing, *J. Supercond. Novel Magn.*, 2014, **27**, 1099.
53 A. Dannenberg, M. Siewert, M. E. Gruner, M. Wuttig and P. Entel, *Phys. Rev. B: Condens. Matter Mater. Phys.*, 2010, **82**, 214421.
54 T. Gasi, V. Ksenofontov, J. Kiss, S. Chadov, A. K. Nayak, M. Nicklas, J. Winterlik, M. Schwall, P. Klaer, P. Adler and C. Felser, *Phys. Rev. B: Condens. Matter Mater. Phys.*, 2013, **87**, 064411.
55 L. Siakeng, G. M. Mikhailov and D. P. Rai, *J. Mater. Chem. C*, 2018, **6**, 10341–10349.
56 D. P. Rai, C. E. Ekuma, A. Boochani, S. Solaymani and R. K. Thapa, *J. Appl. Phys.*, 2018, **123**, 161509.
57 Y. Feng, B. Wu, H. Yuan, A. Kuang and H. Chen, *J. Alloys Compd.*, 2013, **557**, 202–208.
58 A. Ahmad, A. K. Das and S. K. Srivastava, *Eur. Phys. J. B*, 2020, **93**, 96.
59 P. Hohenberg and W. Kohn, *Phys. Rev.*, 1964, **136**, B864–B871.
60 W. Kohn and L. J. Sham, *Phys. Rev.*, 1965, **140**, A1133–A1138.
61 J. P. Perdew, K. Burke and M. Ernzerhof, *Phys. Rev. Lett.*, 1996, **77**, 3865–3868.
62 L. Mikaeilzadeh, A. Tavana and F. Khoeini, *Sci. Rep.*, 2019, **9**, 20075.
63 B. Fadila, M. Ameri, D. Bensaid, M. Noureddine, I. Ameri, S. Mesbah and Y. Al-Douri, *J. Magn. Magn. Mater.*, 2018, **448**, 208–220.
64 X. H. Kang and J. M. Zhang, *J. Phys. Chem. Solids*, 2017, **105**, 9–15.
65 S. A. Khandy, I. Islam, D. C. Gupta, *et al.*, *Sci. Rep.*, 2019, **9**, 1475.
66 K. Nawa and Y. Miura, *RSC Adv.*, 2019, **9**, 30462–30478.
67 C. Zhang, H. Huang, C. Wu, Z. Zhu, Z. He and G. Liu, *Front. Phys.*, 2020, **8**, 232.
68 S. L. Dudarev, G. A. Botton, S. Y. Savrasov, C. J. Humphreys and A. P. Sutton, *Phys. Rev. B: Condens. Matter Mater. Phys.*, 1998, **57**, 1505–1509.
69 D. P. Rai, A. Shankar, Sandeep, L. R. Singh, M. Jamal, S. J. Hashemifar, M. P. Ghimire and R. K. Thapa, *Arm. J. Phys.*, 2012, **5**, 105–110.
70 P. Blaha, K. Schwarz, G. Madsen, D. Kvasnicka, J. Luitz, F. Laskowski, F. Tran and L. D. Marks, *WIEN2K, An Augmented Plane Wave+Local Orbitals Program for Calculating Crystal Structure*, ed. K. Schwarz, Technical University, Wien, Austria, 2018.
71 H. Ebert and J. Minar, *Rep. Prog. Phys.*, 2011, **74**(9), 096501.
72 H. Ebert, *Fully Relativistic Band Structure Calculations for Magnetic Solids - Formalism and Application*, Springer Berlin Heidelberg, Berlin, Heidelberg, 2000, vol. 535, pp. 191–246.
73 Y. I. Matsushita, *et al.*, *J. Phys. D: Appl. Phys.*, 2017, **50**, 095002.
74 M. Gilleben, *et al.*, *J. Comput. Chem.*, 2010, **31**, 612–619.
75 E. S. Popiel, W. Zarek and M. Tuszynski, *Nucleonika*, 2004, **49**, S49–S52.
76 V. Jain, *et al.*, *AIP Conf. Proc.*, 2013, **1536**, 935–936.
77 S. Ghosh and S. Ghosh, *Phys. Scr.*, 2019, **256**, 1900039.
78 M. Meinert, M. P. Geisler, J. Schmalhorst, U. Heinzmann, E. Arenholz, W. Hetaba, M. Stöger-Pollach, A. Hütten and G. Reiss, *Phys. Rev. B: Condens. Matter Mater. Phys.*, 2014, **90**, 085127.
79 K. Endo, H. Matsuda and K. Itoh, *J. Phys. Soc. Jpn.*, 1995, **64**, 2329–2332.
80 H. Luo, Z. Zhu, L. Ma, S. Xu, H. Liu, J. Qu, Y. Li and G. Wu, *J. Phys. D: Appl. Phys.*, 2007, **40**(22), 7121–7127.
81 N. Arıkan, A. İyigör, A. Candan, Ş. Uğur, Z. Charifi, H. Baaziz and G. Uğur, *J. Mater. Sci.*, 2014, **49**(12), 4180–4190.
82 M. Friak, A. Slavik, I. Mihalikova, D. Holec, M. Vsianska, M. Sob, M. Palm and J. Neugebauer, *Materials*, 2018, **11**(9), 1732.
83 F. Dahmane, Y. Mogulkoc, B. Doumi, A. Tadjer, R. Khenata, S. B. Omran, D. P. Rai, G. Murtaza and D. Varshney, *J. Magn. Magn. Mater.*, 2016, **407**, 167–174.
84 F. Aguilera-Granja and R. H. Aguilera-del-Toro, *Mater. Res. Express*, 2019, **6**, 106118.

This journal is © The Royal Society of Chemistry 2020